Electrochimica Acta 258 (2017) 800–806

Contents lists available at ScienceDirect

Electrochimica Acta

journal homepage: www.elsevier.com/locate/electacta

Silicon thin film on graphene coated nickel foam as an anode for Li-ion batteries

Aliya Mukanova [a, b], Arailym Nurpeissova [b], Arshat Urazbayev [b], Sung-Soo Kim [c], Maksym Myronov [d], Zhumabay Bakenov [a, b, e, *]

[a] Department of Chemical Engineering, School of Engineering, Nazarbayev University, 53 Kabanbay Batyr Ave., 010000, Astana, Kazakhstan
[b] National Laboratory Astana, Nazarbayev University, 53 Kabanbay Batyr Ave., 010000, Astana, Kazakhstan
[c] Graduate School of Energy Science and Technology, Chungnam National University, 99 Daehak Ave., Yuseong-gu, Daejeon, 34134, South Korea
[d] Physics Department, University of Warwick, Coventry, CV4 7AL, United Kingdom
[e] Institute of Batteries, 53 Kabanbay Batyr Ave., 010000, Astana, Kazakhstan

ARTICLE INFO

Article history:
Received 9 September 2017
Received in revised form
18 November 2017
Accepted 18 November 2017
Available online 21 November 2017

Keywords:
Silicon anode
Graphene
Thin film anode
Nickel foam
Li-ion battery

ABSTRACT

In this study, we propose a 3D structured composite anode containing silicon thin film on graphene coated Ni foam prepared using chemical vapor deposition and magnetron sputtering techniques. The electrochemical test results show that 3D structure of current collector is capable to effectively suppress/diminish the volume changes of the anode upon cycling. Along with this, graphene serves as an additional electrochemically active component and provides improved conductivity. Designed anode exhibits a high areal capacity of around 75 μAh cm^{-2} upon 500 cycles with the coulombic efficiency of around 99%.

1. Introduction

In spite of being the most powerful technology in secondary batteries, Li-ion batteries (LIBs) cannot meet the demands posed on electrochemical power sources for next generation electric vehicles, mobile electronics and future generations of aircrafts. Currently, energy and power densities of these batteries are limited by the capacity of commonly used anode – graphite, which has a theoretical capacity of 372 mAh g^{-1}.

Silicon (Si) is widely identified as the most promising candidate as a negative electrode for LIBs by virtue of its enormous volume capacity, 9786 mAh cm^{-3}, specific capacity, 4200 mAh g^{-1}, low operating voltage, 0.4 V vs. Li^+/Li, low cost, safety and abundant availability [1]. Despite these advantages, Si has poor electrical conductivity that has to be enhanced in order to achieve high power performance. Unlike graphite, during Li ions insertion to Si proceeds via an alloying mechanism with formation of intermetallic compounds like $Li_{12}Si_7$, Li_7Si_3, $Li_{13}Si_4$ and $Li_{22}Si_5$, which results in a high electric capacity [2–4]. However, this alloying process is encumbered by the huge volume evolution resulting in cracking of Si matrix, and further degradation after a repetitive insertion/extraction processes, leading to the electric contact loss between Si particles and current collector. Eventually, Li alloying and dealloying with Si becomes irreversible, significantly hampering overcharging and reducing energy density.

Several strategies can be employed to improve the performance of Si anode. One of them is to use amorphous Si (a-Si) that preferred in comparison with the crystalline one, which needs a kind of 'activation transformation' to its amorphous state during the initial cycles of lithiation. Moreover, crystalline Si experiences non-uniform expansion due to the presence of crystal lattices resulting in material distortion in a certain direction [5–7]. Another strategy is the application of Si nanopowder, which thought to experience insignificant volume changes during charge/discharge [8]. However, to the best of our knowledge, the efficient and cheap way to produce nanopowder in large scales has not been developed yet. The application of various Si structures like wires [9–11], rods

* Corresponding author. National Laboratory Astana, Department of Chemical Engineering, School of Engineering, Nazarbayev University, 53 Kabanbay Batyr Ave., 010000, Astana, Kazakhstan.
E-mail address: zbakenov@nu.edu.kz (Z. Bakenov).

https://doi.org/10.1016/j.electacta.2017.11.129
0013-4686/

[12], tubes [13,14], trees [15], thin films [16], etc. [17], that are grown on substrates or etched from monolithic Si substrates, is considered as promising as well. In such nanostructures the volume expansion is accommodated due to the available space in the innermost structures, and this extends cycle life of Si anode, although with time, they still experience degradation and capacity fading [16]. The use of an a-Si in the form of thin film, especially with a thickness of no more than 200 nm, significantly improves its lifetime and cycling ability [18]. Unfortunately, low mass loading of Si in these structures does not allow using them in conventional LIBs requiring larger amounts of active material. The attempts to increase the mass of an active Si thin film using shaped substrates (pillars [18], honeycombs [19], lozenge-patterned [20,21], ribbons [22,23], etc.) and Si-based composite thin films (Si/C [24], Si/Cu [25], Si/Fe [26,27], Si/Co [28], Si/B [29], $SiMo_x$ [30], Si/Al [22], Si/LIPON/SnO_2 [31]) were also presented. Applying 3D structured current collectors like metallic nanowires, porous substrates, foams etc. [32,33] could be considered as one of promising approaches to overcome limited materials load problem of thin film silicon anode. In fact, this design strategy is the only route to obtain a well operating Si anode in which 3D current collector provides high surface-to volume ratio for electrochemical interaction, electrical network for enhanced conductivity as well as space reservoirs to accommodate the volume changes of the anode upon operation. In order to enhance the electron mobility in electrode and to, subsequently, improve the battery performance, the n- or p-type dopants can be easily incorporated in the material during preparation of the Si film [34–36].

Graphene is a material that often used as a conductive additive in positive and negative electrodes [37]. Besides, graphene can be used to prepare a free-standing anode material with a low discharge potential and a high theoretical specific capacity of 744 mAh g^{-1} owing to its ability for double-site lithiation (LiC_3) [38,39]. Moreover, Paronyan et al. reported on pure graphene-based anodes with ability to deliver a capacity over 1116 mAh g^{-1} due to lithium ions occupation of the adjacent sites of graphene sheets with formation of LiC_2 intercalates [40].

Inspired by these works, herein, we report for the first time on design of novel electrode material, the n-doped a-Si thin film on graphene (GF) coated nickel (Ni) foam as anode for LIBs. Ni foam is able to produce defect free GF layers as it was reported before [41] with increased surface area of the sheets. Chemical vapor deposition (CVD) and magnetron sputtering (MS) were utilized to obtain the targeted electrode material.

2. Experimental

2.1. Material synthesis

2.1.1. Graphene film synthesis

A CVD growth of GF was implemented onto Ni foam, which served as a 3D interconnected substrate with a catalytic ability to absorb and release carbon atoms facilitating them to arrange into a hexagonal lattice in the spaces between Ni atoms [42]. Ni foam was purchased from Goodfellow Inc. and had the following parameters: the thickness of foam was 1.6 mm, the porosity of more than 95% with the mean hole diameter of 0.22 mm. Prior to CVD, heat treatment of Ni foam was carried out in a high temperature furnace STF1200 (Across International) in a mixture of argon and hydrogen (95% Ar + 5% H_2) with preheating at 200 °C during 30 min to remove the moisture from the catalyst surface and further at 1020 °C to remove the rest of contaminations and to reduce the native NiO layer to Ni. After this, the precursor gas, a methane-containing gas mixture (90% Ar + 10% CH_4), was injected into the furnace. In order to obtain a few layer GF, the inlet of gas lasted for 5 min only (ambient pressure). Carbon atoms that were absorbed by Ni, released during cooling, forming a high quality few layer GF [43]. The CVD schematics is presented in Fig. 1a, and the experiment conditions are summarized in Table 1. The mass increment of samples was controlled using weighting by an ultra-microbalance (Sartorius, MSE2.7S-000-DM) and constituted around 0.41 ± 0.02 mg cm^{-2} and almost equal for all samples. Prior to CVD and magnetron sputtering all Ni foam samples were cleaned by diluted HCl (1:1 v/v), followed by rinsing with deionized water.

2.1.2. Silicon thin film sputtering

The Si thin film was deposited onto one side of GF-Ni by magnetron sputtering (Kurt J. Lesker Inc.), as illustrated in Fig. 1b. During sputtering, an n-type doped Si target (99.99%) was hit by Ar ions, generated between two magnets. This process led to emission of target atoms and their deposition on the substrate. The main advantage of MS is easiness of the process along with a capability to prepare amorphous Si with high purity as well as easy control of the film thickness. The synthesis conditions (Table 1) were chosen based on the literature data. In particular, the power mode (*rf*) and magnitude of 80 W employed in this work was adopted from Omampuliyur et al. [18] who has determined the optimal power to prepare Si thin film with certain density and low oxygen content. The sputtering was carried out at an angle 30° in order to ensure that the target ions might be able to reach the innermost whisks of the foam substrate. The mass increment of Si constituted around 0.04 ± 0.002 mg cm^{-2} for both Si-Ni and Si-GF-Ni samples, and was determined by weighing the samples before and after sputtering by an ultra-microbalance.

2.2. Material characterization

The structure of GF and Si were examined by Raman spectroscopy on a LabRAM HR Evolution spectrometer (HORIBA Scientific) using Ar ion excitation laser of 532 nm. The morphology of samples' surface was observed by scanning electron microscope (SEM, Zeiss Crossbeam 540) before and after electrochemical cycling at a voltage of 4 kV. The uniformity of GF layer on Ni was studied using SEM combined with energy dispersive spectroscope EDS TM3030 (Hitachi) at a voltage of 15 kV. Prior to microscopic observation the electrodes extracted from the disassembled cells were immersed into diethylene carbonate (DEC) solvent for several days to remove all carbonate components of a solid electrolyte interphase (SEI) layer followed by meticulous rinsing in ethanol and drying.

2.3. Cell assembly and electrochemical measurements

Before assembling the cells, the anodes were annealed in a mixture gas Ar + (5%) H_2 (flow rate of 150 cm^3 min^{-1}) in a high temperature tubular furnace STF 1200 (Across International Inc., USA) at 150 °C for 60 min to remove condensed moisture from the surface, and then at 300 °C for 60 min in order to remove oxides. Due to the interdiffusion of Si and Ni or C at the interface between two layers, annealing strengthens the adhesion between the Si film and the substrate. This is known to positively affect the performance of the batteries [44].

The electrode was studied in a 2032 type coin cell using a lithium metal foil as a counter and reference electrode, a commercial 1 M $LiPF_6$ in ethylene/diethyl/ethyl methyl carbonates (EC: DEC: EMC, 1:1:1 v/v) as an electrolyte solution and a polypropylene membrane (Celgard® 2400) as a separator. The cells were assembled in a glove box filled with Ar (MBRAUN, LABmaster Pro Glovebox, Germany, <0.1 ppm H_2O and O_2). The batteries with Si-GF-Ni and Si-Ni electrodes were tested by cyclic voltammetry (CV) and galvanostatic cycling using a potentiostat/galvanostat (VMP3,

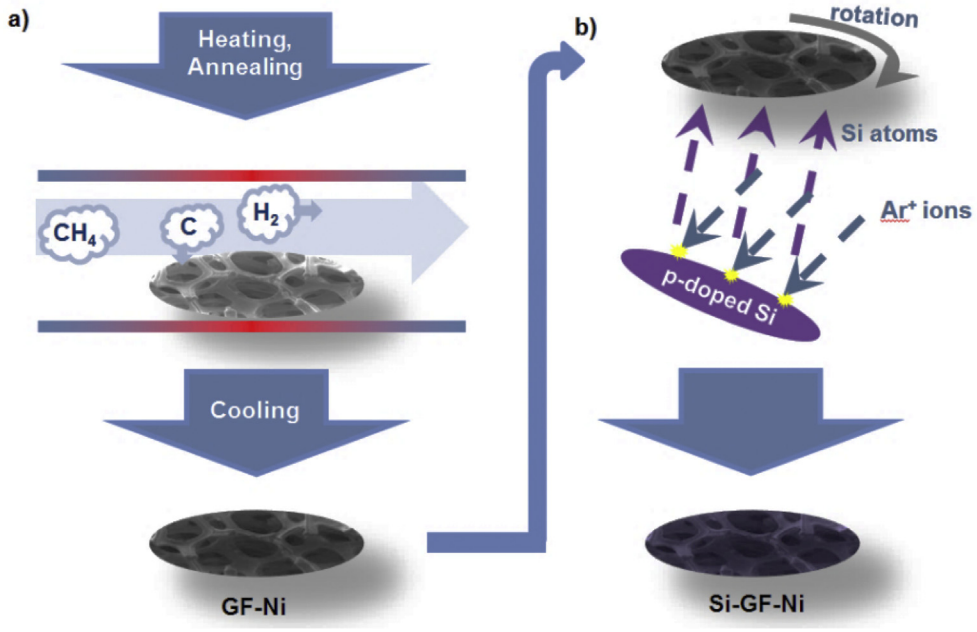

Fig. 1. Schematic view of experiments: (a) CVD, (b) MS.

Table 1
Conditions of CVD and MS processes.

CVD			MS	
Gas	Ar + H_2 (5% + 95%)		Gas	Ar (99%)
Gas flow	100 sccm		Pressure	5 mTorr
Precursor	CH_4+Ar (7% + 93%)		Target	n-type doped Si (99.99%)
Steps	Annealing	200 °C, 60 min	Power	Rf, 80 W
	Annealing	1020 °C, 60 min, 300 sccm (Ar + H_2)	Rotation	5 rpm
	Deposition	1020 °C, 5 min, 220 sccm (Ar + CH_4)+300 sccm (Ar + H_2)	Temperature	room
Cooling		Naturally	Time	60 min

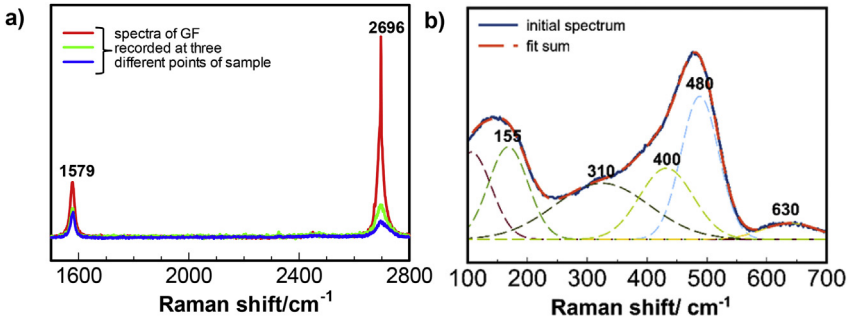

Fig. 2. Raman spectra of samples: (a) graphene, (b) Si thin film.

Biologic Inc.) and a multichannel battery testing system (Arbin Inc.). CV was measured in a potential range of 0–3 V at a scan rate of 0.1 mV s^{-1}; galvanostatic cycling was performed between 0.1 and 1.5 V at a current density of 30 μAh cm^{-2}. In order to avoid the errors related to the low mass of the electrodes, the results were presented as an areal capacity (μAh cm^{-2}), however, the approximate specific capacities are also given. All potentials are presented *vs.* Li^+/Li.

3. Results and discussion

Raman spectra of the GF thin film and Si thin film coated on Ni foam are shown in Fig. 2. The spectra for GF (Fig. 2a) represent the results taken from the same sample at three different measurement points. All three spectra display similar scattering patterns presented by two peaks at around 1579 cm^{-1} and 2696 cm^{-1} assigned to the G and 2D bands of carbon materials, respectively. A missing D band (~1320 cm^{-1}) evidences a high purity and well-ordered structure of the synthesized GF. In order to determine the number of the graphene layers, the spectra were analyzed as follows. Single and bilayer GF sheets usually have a ratio of 2D to G bands' intensities more than 3 [45]. In our case, the record of scattering response on three different points resulted in various intensities consequently leading to various 2D/G ratio from 0.75 to 3.2. Full

width half maximum (FWHM) of the G band can also provide information about the number of GF layers. According to literature data, for a monolayer of GF a FWHM constitutes 20-30 cm^{-1}, while for a four and five layered graphene this value is around 70 cm^{-1} [46]. The calculated FWHM for our sample is within a range of 20–80 cm^{-1}. Thus, on a basis of Raman spectroscopy plots we can suppose that the carbon film synthesized on Ni foam is a few layered GF with high purity and quality. From Fig. 2b, we can detect that the Raman spectrum for Si thin film does not exhibit a typical crystalline band usually located at a shift position of 520 cm^{-1}. Instead, several components of the spectrum can be easily distinguished by a simple fitting: transverse optic and acoustic modes at 480 cm^{-1} and 155 cm^{-1}, respectively, and longitudinal optic and acoustic modes at 400 cm^{-1} and 310 cm^{-1}, respectively. One more peak at 630 cm^{-1} is ascribed to the second order of longitudinal acoustic mode and overtone of transverse acoustic and optical modes. These peaks match well with those of Si amorphous phase [29].

The microstructural morphologies of the as-prepared samples were revealed by SEM. The results of these studies are presented in Fig. 3, which demonstrates the surface of Ni foam and its cells walls/wires after cleaning with acetone. In a higher resolution images, incorporated into Fig. 3, one can see the distinguishable surface grain boundaries. Fig. 3b illustrates the sample after CVD, on which a dark film, consisting of numerous GF sheets, can be detected on the Ni foam surface. GF layers replicate the shape of boundaries over the Ni foam surface. Fig. 3c depicts images of Si thin film with an inset image of a higher magnification. We can clearly see the dense thin film composed of interconnected nanosized spherical particles with the diameters of up to 100 nm. The dimensions and shapes are identical for both samples, Si-Ni and Si-G-Ni. Due to complicated structure of substrate and deposition technique, it is hard to provide the mean value of Si thin film thickness, however the observed range of thicknesses was between 50 and 150 nm.

The SEM/EDX scans demonstrate the surfaces of as-deposited GF-Ni samples and the C and Ni elements distribution map (Fig. 4). It can be seen that carbon and nickel are uniformly distributed in the sample. In the EDX results, only C and Ni peaks could be recorded. From the distribution map of carbon, one can see some dark spots with no carbon, which might be an indication of delamination of GF sheets from the substrate within these spots.

In order to further study the beneficial effects of prepared materials as anodes for LIBs, their electrochemical performance was examined in lithium half-cells. Fig. 5 shows CVs of the samples measured at a scan rate of 0.01 V s^{-1} within a potential range 0–3 V. The CV plots of 3D Si-Ni anode are illustrated in Fig. 5a. Distinguishable cathodic peaks observed at around 1.37 V and 0.4 V during the initial discharge process can be ascribed to the first occurred reactions between lithium ions and electrolyte on a NiO native layer of Ni foam [47] and on the surface of Si [47], respectively, with the formation of solid electrolyte interphase (SEI) on the electrode surface. Another cathodic peak at around 0.84 V is related to the reaction between Li ions and NiO native layer of Ni foam where NiO reduces to Ni and Li_2O forms [48,49]. The next process is alloying of lithium ions into Si thin film (Li_xSi_y) at the potentials of 0.012 V and 0.001 V with the posterior dealloying at 0.33 V and 0.53 V, which corresponds to a release of lithium ions from Li_xSi_y alloy during the discharge stage. The anodic peak of around 1.3 V can be ascribed to a reversible reaction between Ni and Li_2O [48,49]. Fig. 5b shows the CV curves of Si-GF-Ni anode. An initial SEI layer formation on GF surface can be indicated by a small peak at around 0.7 V, disappearing in the following cycles. The lithiation reaction of GF extends the peak intensity at around 0.01 V as well as that of its corresponding delithiation peak at around 0.3 V. The reaction governing the first delithiation peak of Si usually occurs at the same potential [50,51]. Besides, the second Si delithiation peak at 0.49 V is observed on the anodic scans, indicating the participation of Si in the overall electrochemical reaction. It is noticeable in the magnified graph in Fig. 5b that the NiO lithiation/delithiation peaks are still present in Si-GF-Ni electrode indicating that the native oxide layer was not completely removed from Ni foam surface.

Fig. 6 shows the results of galvanostatic charge/discharge cycling of the Si-Ni and Si-GF-Ni anodes performed at a current

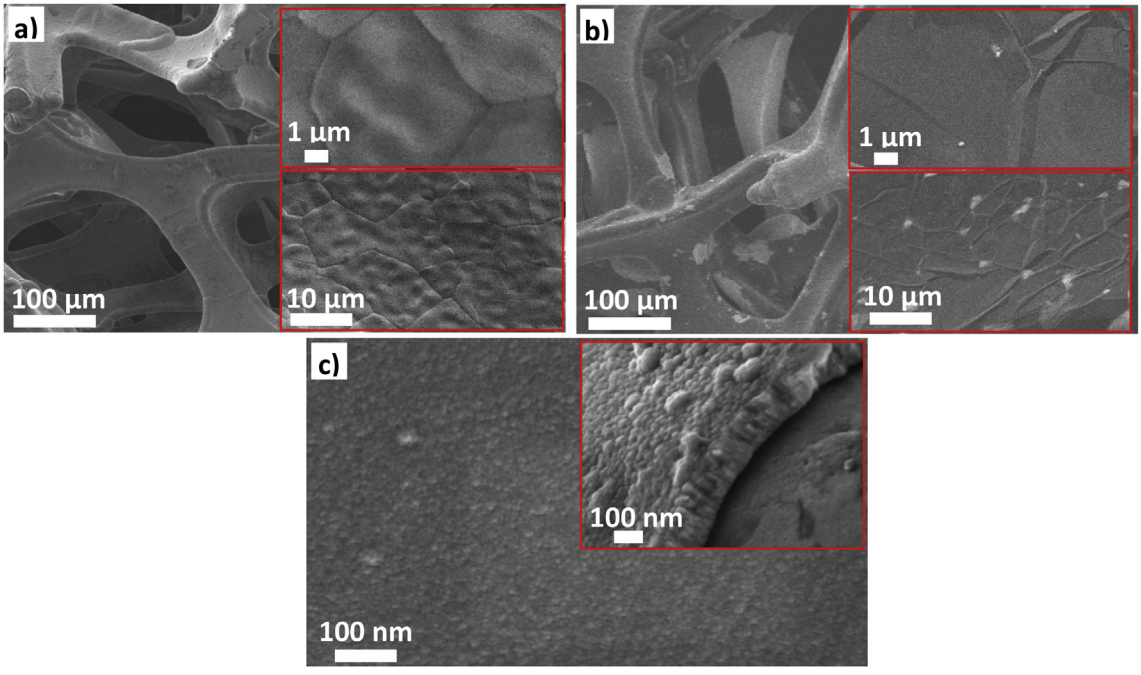

Fig. 3. SEM images of (a) pristine Ni foam, (b) GF deposited on Ni, and (c) sputtered Si thin film.

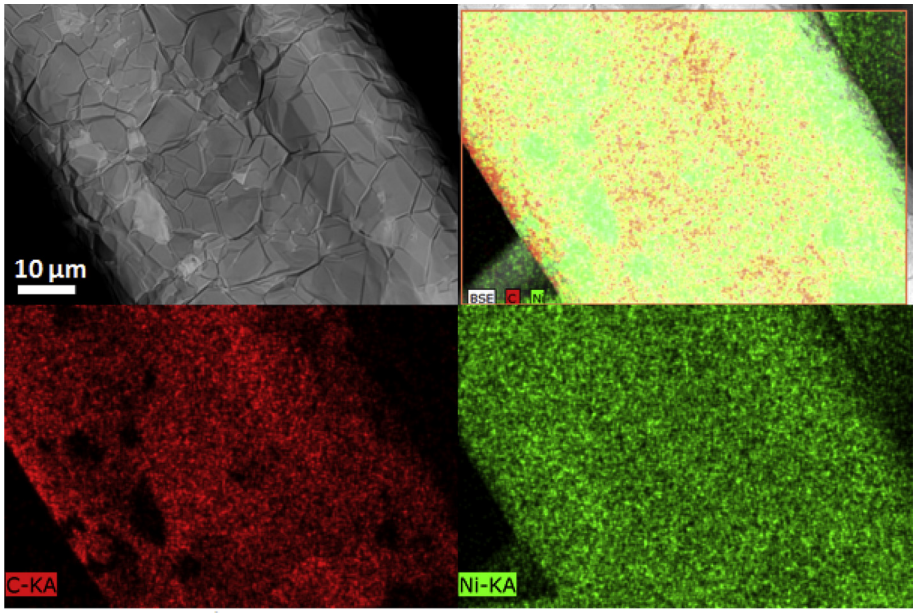

Fig. 4. Results of SEM/EDX analysis of the GF-Ni sample.

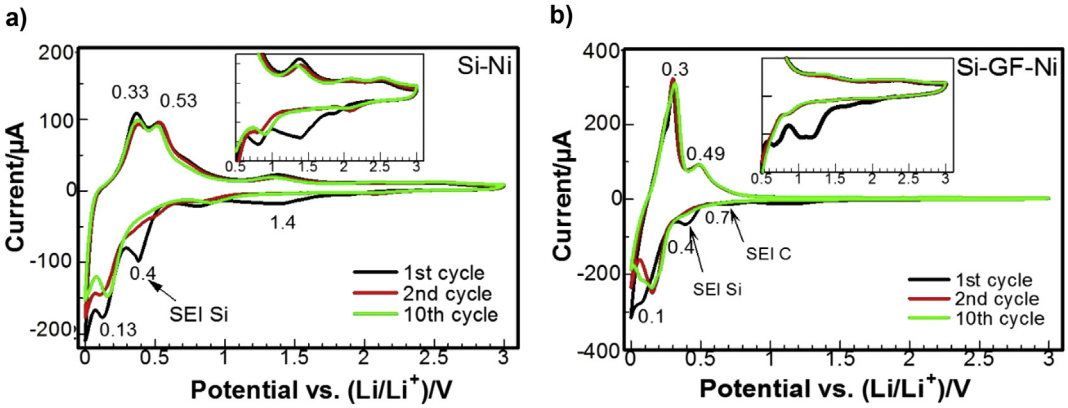

Fig. 5. CV plots of (a) Si- Ni, and (b) Si-GF-Ni.

density of 30 µA cm^{-2} within a potential window of 0.1–1.5 V. All plateaus on charge/discharge curves correspond to the lithiation/delithiation potentials observed in the CV plots above. From Fig. 6a, we can detect that Si thin film on pure Ni loses almost a half of its initial discharge capacity of 93 µAh cm^{-2} after the 1st cycle and experiences a gradual capacity fading up to the final recorded cycle. The Si-GF-Ni anode exhibits a higher initial areal capacity of around 141 µAh cm^{-2} which stabilizes at about 80 µAh cm^{-2} within 10 cycles (Fig. 6b). If the retained capacities of the anodes are presented in the specific gravimetrical units, Si-Ni exhibits a capacity of 2318/1245 mAh g^{-1} in the initial discharge/charge and 296/296 mAh g^{-1} at the last 500th cycle, respectively. On the other hand, Si-GF-Ni delivers a capacity of only 326/225 mAh g^{-1} and 175/175 mAh g^{-1} in the first and last discharge/charge, respectively, which is due to a low content of Si about 9%. However, it should be noted that Si delivers about half of this capacity of the composite anode. Comparing the cycling performance of Si-Ni and Si-GF-Ni presented in Fig. 6c, it can be noted that the Si-Ni anode system exhibits a poor capacity retention, and it drastically fades upon cycling. Meanwhile, the Si-GF-Ni anode maintains the areal capacity within a range of 70–80 µAh cm^{-2} upon all 500 cycles performed. The improved performance could be resulted from electrochemical activity of GF towards Li-ions.

Fig. 7 illustrates SEM images of the samples retracted from the cells cycled 500 times. The post-cycling investigations of Si-Ni anode (Fig. 7a) revealed the presence of cracks and partial delamination of Si thin film from Ni foam. Besides, this detachment is not so wide as for flat monolithic Si thin films reported earlier [7]. From SEM images of Si-GF-Ni shown in Fig. 7b, we detected an extensive delamination of graphene sheets together with the sputtered Si thin film. In spite of this, designed anode system did not have any failure in maintaining its capacity. We suppose, that this can be explained by the fact that GF provides an improved substrate adhesion for Si thin film.

The designed 3D compositional Si-GF-Ni electrode showed a promising potential for use in LIBs owing to a combination of two active materials in one system. In fact, this is the first step towards designing this high performance system, and further improvement will be directed in achieving more stable GF underlayer, removing Ni scaffold and obtaining a-Si thin film covering the whole surface of GF in order to increase the active mass loading and, consequently, the specific capacity of the composite thin film. Besides,

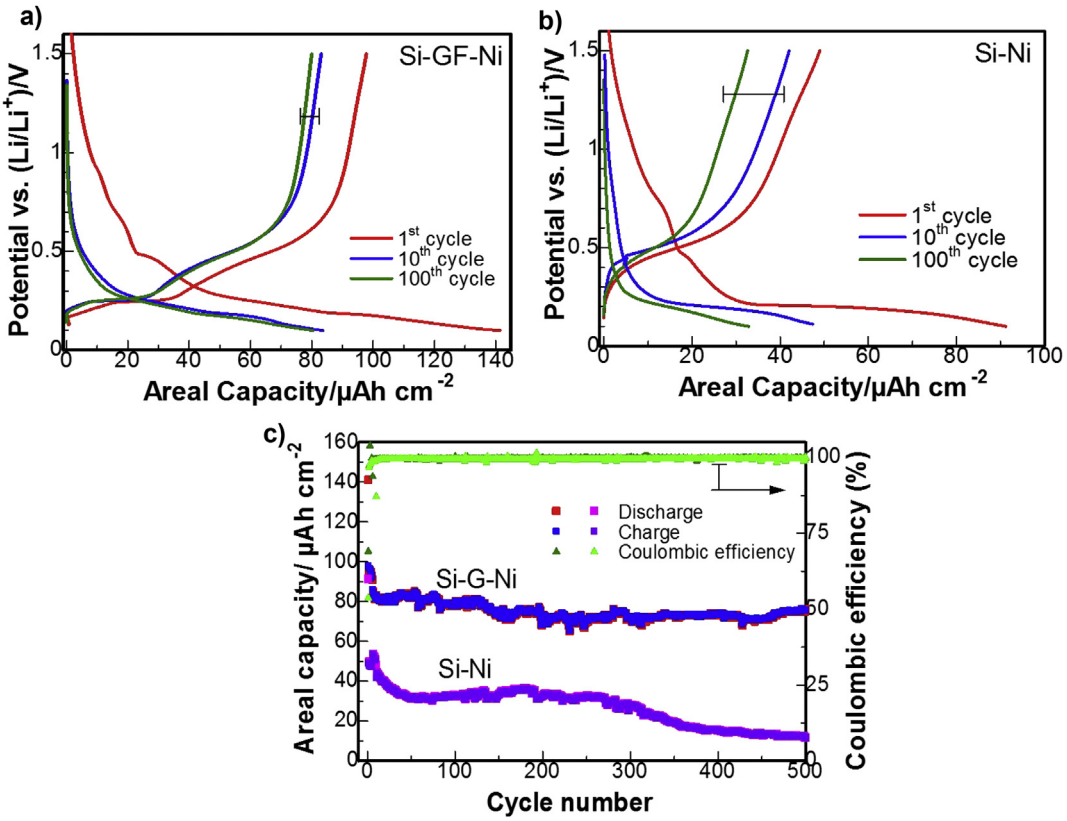

Fig. 6. Charge/discharge curves of (a) Si-Ni, (b) Si-GF-Ni, and (c) cycling performance of both Si-Ni and Si-GF-Ni anodes.

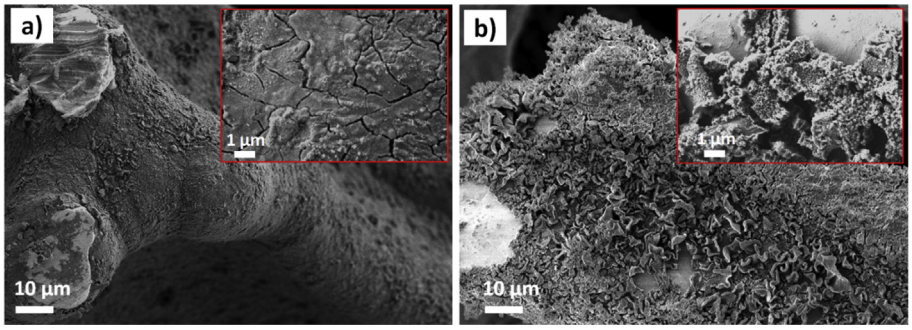

Fig. 7. SEM images of the samples after 500 cycles (a) Si-Ni, (b) Si-GF-Ni.

the mass of the anode will be significantly reduced by removing the metallic substrate and forming a free-standing anode film. The presence of GF will serve as a guarantee for backup the anode operation even in case of Si degradation upon a long term cycling. It is especially important in special cases such as medical and some other electronics devices, where the immediate battery failure may stop vital processes.

4. Conclusion

In this work, a facile strategy to produce compositional 3D Si-GF-Ni anode system was presented. The suggested anode system comprises a combination of strategies such as the use of 3D current collector, thin film structure of Si, magnetron sputtering derived amorphous phase of Si and n-type dopants incorporation, and CVD grown graphene on the surface of Ni foam. We suggest that the presence of the graphene component in the electrode has significantly improved the performance of Si thin film anode due to its electrochemical activity towards Li ions, high electronic conductivity and enhanced adhesion for Si thin film. As a result, the designed electrode with n-type doped Si film and GF on Ni foam retained a stable areal capacity of around 75 μAh cm^{-2} over 500 cycles with a slow capacity loss of 0.01 μAh cm^{-2} per cycle and a coulombic efficiency as high as 99.5%. The current research provides an effective approach towards further enhanced design of a high-performance system with a two active components combination, which could be modified to freestanding lightweight Si-GF anode for thin film and conventional LIBs.

Acknowledgments

The authors acknowledge financial support from the Ministry of Education and Science of the Republic of Kazakhstan (the Targeted Program No. 0115PK03029 “NU-Berkeley strategic initiative in

warm-dense matter, advanced materials and energy sources for 2014–2018", research grants 5097/GF4-1 "Development of a novel quartz (SiO2) based composite anode material for Li-ion batteries" and 4649/GF4-8 "Development of economically feasible three-dimensional lithium/sulfur battery").

References

[1] N. Nitta, G. Yushin, High-capacity anode materials for lithium-ion batteries: choice of elements and structures for active particles, Part. Part. Syst. Charact. 31 (2014) 317–336.

[2] T.D. Hatchard, J.R. Dahn, In Situ XRD and electrochemical study of the reaction of lithium with amorphous silicon, J. Electrochem. Soc. 151 (2004) A838–A842.

[3] D. Ma, Z. Cao, A. Hu, Si-based anode materials for li-ion batteries: a mini review, Nano-Micro Lett. 6 (2014) 347–358.

[4] P. Limthongkul, Y. Il Jang, N.J. Dudney, Y.M. Chiang, Electrochemically-driven solid-state amorphization in lithium-metal anodes, J. Power Sources 119–121 (2003) 604–609.

[5] A. Casimir, H. Zhang, O. Ogoke, J.C. Amine, J. Lu, G. Wu, Silicon-based anodes for lithium-ion batteries: effectiveness of materials synthesis and electrode preparation, Nano Energy 27 (2016) 359–376.

[6] S. Bourderau, T. Brousse, D. Schleich, Amorphous silicon as a possible anode material for Li-ion batteries, J. Power Sources 81–82 (1999) 233–236.

[7] J.P. Maranchi, A.F. Hepp, P.N. Kumta, High capacity, reversible silicon thin-film anodes for lithium-ion batteries, Electrochem. Solid-State Lett. 6 (2003) A198.

[8] X.H. Liu, L. Zhong, S. Huang, S.X. Mao, T. Zhu, J.Y. Huang, Size-dependent fracture of silicon nanoparticles during lithiation, ACS Nano 6 (2012) 1522–1531.

[9] W. Xu, Silicon Nanowire Anode for Lithium-ion Batteries: Fabrication, Characterization and Solid Electrolyte Interphase, Louisiana State University and Agricultural and Mechanical College, 2011.

[10] P.P. Prosini, M. Carewska, F. Maroni, R. Tossici, F. Nobili, A lithium-ion battery based on LiFePO4 and silicon/reduced graphene oxide nanocomposite, Solid State Ionics 283 (2015) 145–151.

[11] M. Ge, J. Rong, X. Fang, C. Zhou, Porous doped silicon nanowires for lithium ion battery anode with long cycle life, Nano Lett. 12 (2012) 2318–2323, https://doi.org/10.1021/nl300206e.

[12] D. Zschech, D.H. Kim, A.P. Milenin, R. Scholz, R. Hillebrand, C.J. Hawker, T.P. Russell, M. Steinhart, U. Gösele, Ordered arrays of <100>-oriented silicon nanorods by CMOS-compatible block copolymer lithography, Nano Lett. 7 (2007) 1516–1520.

[13] Z. Wen, G. Lu, S. Mao, H. Kim, S. Cui, K. Yu, X. Huang, P.T. Hurley, O. Mao, J. Chen, Silicon nanotube anode for lithium-ion batteries, Electrochem. Commun. 29 (2013) 67–70.

[14] H. Wu, G. Chan, J.W. Choi, I. Ryu, Y. Yao, M.T. McDowell, S.W. Lee, A. Jackson, Y. Yang, L. Hu, Y. Cui, Stable cycling of double-walled silicon nanotube battery anodes through solid–electrolyte interphase control, Nat. Nanotechnol. 7 (2012) 310–315.

[15] L. Leveau, B. Laïk, J.P. Pereira-Ramos, A. Gohier, P. Tran-Van, C.S. Cojocaru, Silicon nano-trees as high areal capacity anodes for lithium-ion batteries, J. Power Sources 316 (2016) 1–7.

[16] U. Kasavajjula, C. Wang, A.J. Appleby, Nano- and Bulk-silicon-based Insertion Anodes for Lithium-ion Secondary Cells, vol. 163, 2007, pp. 1003–1039.

[17] L. Liu, J. Lyu, T. Li, T. Zhao, L. Liu, J. Lyu, T. Li, T. Zhao, Well-constructed silicon-based materials as high-performance lithium-ion battery anodes, Nanoscale 8 (2016) 701.

[18] R.S. Omampuliyur, M. Bhuiyan, Z. Han, Z. Jing, L. Li, E.A. Fitzgerald, C.V. Thompson, W.K. Choi, Nanostructured thin film silicon anodes for Li-Ion microbatteries, J. Nanosci. Nanotechnol. 15 (2015) 4926–4933.

[19] L. Baggetto, D. Danilov, P.H.L. Notten, Honeycomb-structured silicon: remarkable morphological changes induced by electrochemical (De)lithiation, Adv. Mater. 23 (2011) 1563–1566.

[20] G.B. Cho, J.P. Noh, H.J. Sung, S.Y. Choi, S.H. Lee, H.J. Ahn, T.H. Nam, K.W. Kim, Improved electrochemical properties of patterned Si film electrodes, Microelectron. Eng. 89 (2012) 104–108.

[21] G. Cho, J. Noh, H. Sung, S. Lee, Y. Im, H. Ahn, K. Kim, Patterned Si thin film electrodes for enhancing structural stability, Nanoscale Res. Lett. 7 (2012) 20.

[22] Q. Zhang, J. Liu, Z.Y. Wu, J.T. Li, L. Huang, S.G. Sun, 3D nanostructured multilayer Si/Al film with excellent cycle performance as anode material for lithium-ion battery, J. Alloys Compd. 657 (2016) 559–564.

[23] H.-C. Shin, J. a. Corno, J.L. Gole, M. Liu, Porous silicon negative electrodes for rechargeable lithium batteries, J. Power Sources 139 (2005) 314–320.

[24] M.K. Datta, J. Maranchi, S.J. Chung, R. Epur, K. Kadakia, P. Jampani, P.N. Kumta, Amorphous silicon-carbon based nano-scale thin film anode materials for lithium ion batteries, Electrochim. Acta 56 (2011) 4717–4723.

[25] H.J. Ahn, Y.S. Kim, W.B. Kim, Y.E. Sung, T.Y. Seong, Formation and characterization of Cu-Si nanocomposite electrodes for rechargeable Li batteries, J. Power Sources 163 (2006) 211–214.

[26] J.B. Kim, H.Y. Lee, K.S. Lee, S.H. Lim, S.M. Lee, Fe/Si multi-layer thin film anodes for lithium rechargeable thin film batteries, Electrochem. Commun. 5 (2003) 544–548.

[27] J.B. Kim, B.S. Jun, S.M. Lee, Improvement of capacity and cyclability of Fe/Si multilayer thin film anodes for lithium rechargeable batteries, Electrochim. Acta 50 (2005) 3390–3394.

[28] X.H. Huang, J.B. Wu, Y.Q. Cao, P. Zhang, Y. Lin, R.Q. Guo, Cobalt nanosheet arrays supported silicon film as anode materials for lithium ion batteries, Electrochim. Acta 203 (2016) 213–220.

[29] V. Baranchugov, E. Markevich, E. Pollak, G. Salitra, D. Aurbach, Amorphous silicon thin films as a high capacity anodes for Li-ion batteries in ionic liquid electrolytes, Electrochem. Commun. 9 (2007) 796–800.

[30] C.M. Hwang, C.H. Lim, J.H. Yang, J.W. Park, Electrochemical properties of negative SiMox electrodes deposited on a roughened substrate for rechargeable lithium batteries, J. Power Sources 194 (2009) 1061–1067.

[31] J. Lin, J. Guo, C. Liu, H. Guo, Artificial solid electrolyte interphase with in-situ formed porosity for enhancing lithiation of silicon wafer, J. Power Sources 336 (2016) 401–407.

[32] K.L. Lee, J.Y. Jung, S.W. Lee, H.S. Moon, J.W. Park, Electrochemical characteristics of a-Si thin film anode for Li-ion rechargeable batteries, J. Power Sources 129 (2004) 270–274.

[33] R. Lin, S. Zhang, Z. Du, H. Fang, Y. Ren, X. Wu, Copper nanowires based current collector for light-weight and flexible composite silicon anode with high stability and specific capacity, RSC Adv. 5 (2015) 87090–87097, https://doi.org/10.1039/C5RA13568K.

[34] T. Takamura, S. Ohara, M. Uehara, J. Suzuki, K. Sekine, A vacuum deposited Si film having a Li extraction capacity over 2000 mAh/g with a long cycle life, J. Power Sources 129 (2004) 96–100.

[35] J.K. Lee, J.O. Song, H.T. Shim, D.J. Byun, A study on the effect of structure and P-doping of Si thin film as an anode for lithium rechargeable batteries, Adv. Nanomater. Process 124–126 (2007) 1063–1066. Pts 1 2.

[36] A.A. Arie, J.K. Lee, Electrochemical properties of P-doped silicon thin film anodes of lithium ion batteries, 737, 2013, pp. 80–84.

[37] J. Wei, Z. Zang, Y. Zhang, M. Wang, J. Du, X. Tang, Enhanced performance of light-controlled conductive switching in hybrid cuprous oxide/reduced graphene oxide (Cu2O/rGO) nanocomposites, Opt. Lett. 42 (2017) 911–914.

[38] H. Sun, A.E.D.R. Castillo, S. Monaco, A. Capasso, A. Ansaldo, M. Prato, D.A. Dinh, V. Pellegrini, B. Scrosati, L. Manna, F. Bonaccorso, Binder-free graphene as advanced anode for lithium batteries Haiyan, J. Mater. Chem. A 4 (2016) 6886–6895.

[39] F.J. Sonia, M.K. Jangid, B. Ananthoju, M. Aslam, P. Johari, A. Mukhopadhyay, Understanding the Li-storage in few layers graphene with respect to bulk graphite: experimental, analytical and computational study †, J. Mater. Chem. A Mater. Energy Sustain 5 (2017) 8662–8679.

[40] T.M. Paronyan, A.K. Thapa, A. Sherehiy, J.B. Jasinski, J.S.D. Jangam, Incommensurate graphene foam as a high capacity lithium intercalation anode, Sci. Rep. 7 (2017) 39944.

[41] S. Amini, J. Garay, G. Liu, A.A. Balandin, R. Abbaschian, S. Amini, J. Garay, G. Liu, A.A. Balandin, Growth of Large-area Graphene Films from Metal-carbon Melts Growth of Large-area Graphene Films from Metal-carbon Melts, 2010, p. 94321.

[42] Z. Chen, W. Ren, L. Gao, B. Liu, S. Pei, H. Cheng, Three-dimensional flexible and conductive interconnected graphene networks grown by chemical vapour deposition, Nat. Mater. 10 (2011) 424–428.

[43] L. Baraton, Z.B. He, C.S. Lee, C.S. Cojocaru, M. Châtelet, J.-L. Maurice, Y.H. Lee, D. Pribat, On the Mechanisms of Precipitation of Graphene on Nickel Thin Films, vol. 1, 2011, pp. 1–6.

[44] L.B. Chen, J.Y. Xie, H.C. Yu, T.H. Wang, An amorphous Si thin film anode with high capacity and long cycling life for lithium ion batteries, J. Appl. Electrochem 39 (2009) 1157–1162.

[45] S. Thiele, A. Reina, P. Healey, J. Kedzierski, P. Wyatt, P.-L. Hsu, C. Keast, J. Schaefer, J. Kong, Engineering polycrystalline Ni films to improve thickness uniformity of the chemical-vapor-deposition-grown graphene films, Nanotechnology 21 (2010) 15601.

[46] Y. Hao, Y. Wang, L. Wang, Z. Ni, Z. Wang, R. Wang, C.K. Koo, Z. Shen, J.T.L. Thong, Probing layer number and stacking order of few-layer graphene by raman spectroscopy, Small 6 (2010) 195–200.

[47] C. Li, C. Liu, W. Wang, Z. Mutlu, J. Bell, K. Ahmed, R. Ye, M. Ozkan, C.S. Ozkan, Silicon derived from glass bottles as anode materials for lithium ion full cell batteries, Sci. Rep. (2017) 1–11.

[48] G. Evmenenko, T.T. Fister, D.B. Buchholz, Q. Li, K.S. Chen, J. Wu, V.P. Dravid, M.C. Hersam, P. Fenter, M.J. Bedzyk, Morphological evolution of multilayer Ni/NiO thin film electrodes during lithiation, ACS Appl. Mater. Interfaces 8 (2016) 19979–19986.

[49] P. Poizot, S. Laruelle, S. Grugeon, L. Dupont, J. Tarascon, Nano-sized transition-metal oxides as negative-electrode materials for lithium-ion batteries, Nature 407 (2000) 496–499.

[50] A.P. Cohn, L. Oakes, R. Carter, S. Chatterjee, A.S. Westover, K. Share, C.L. Pint, Assessing the improved performance of freestanding, flexible graphene and carbon nanotube hybrid foams for lithium ion battery anodes, Nanoscale 6 (2014) 4669.

[51] F. Ding, W. Xu, D. Choi, W. Wang, X. Li, M.H. Engelhard, X. Chen, Z. Yang, J.-G. Zhang, Enhanced performance of graphite anode materials by AlF3 coating for lithium-ion batteries, J. Mater. Chem. 22 (2012) 12745.